Effect of LHC data on Extensive Air Shower Development

T. Pierog

Karlsruhe Institute of Technology (KIT), IKP, D-76021 Karlsruhe, Germany

The uncertainty in the prediction of shower observables for different primary particles and energies is currently dominated by differences between hadronic interaction models. Since the end of 2009, LHC data have become available for proton-proton scattering at different energies, extending the reach of collider data. The LHC data on minimum bias measurements has been used to test and improve Monte Carlo generators and these new constrains reduce the uncertainties in air shower predictions. In this contribution, we will show the results of the comparison between the newly available hadronic interaction models EPOS LHC and QGSJETII-04 and LHC data. Implications for air shower simulations will be discussed.

1 Introduction

Most of the Astronomy and Astrophysics is done using electromagnetic signals from radio to gamma rays. It gives precious informations on the various objects observed in the Universe and their history. In fact a part of these signals is produced by elementary charged particles like electrons or nuclei which can escape the source and reach the Earth after a long propagation through the (extra)galactic medium. Eventually these charged particles may cross the path of the Earth and enter our field of view: they are cosmic rays. Due to the steeply falling energy spectrum of cosmic rays, direct detection by satellite- or balloon-borne instruments is only possible up to about $\sim 10^{14}$ eV. Fortunately, at such high energies, the cascades of secondary particles produced by cosmic rays reach the ground and can be detected in coincidence experiments. The cascades are called extensive air showers (EAS) and are routinely used to make indirect measurements of high energy cosmic rays. The upper limit of the detectable energy is given by the area and exposure time of the detector. For instance, the Pierre Auger Observatory (PAO)[1], which is currently taking data in Argentina, is designed to detect particles of $\sim 10^{20}$ eV for which the flux is less than one particle per km^2 and century.

As a consequence of the indirect character of the measurement, detailed simulations of air showers are needed to extract information on the primary particle from shower observables. Indeed the cascade is initiated by a first hadronic interaction between the initial charged primary cosmic ray and one nucleus from the atmosphere. After their propagation limited by their cross section, the secondary hadronic particles will interact again forming the hadronic cascade which is the skeleton of the EAS. At each hadronic interaction about one third of the energy goes into the π^0 which immediately decay into two photons feeding the electromagnetic cascade. After few hadronic generations, more than 90% of the energy of the primary particle is carried by the electromagnetic component of the EAS. Whereas electromagnetic interactions are well understood within perturbative QED, hadronic multi-particle production cannot be calculated within QCD from first principles. Differences in modelling hadronic interactions, which cannot be resolved by current accelerator data, are the main source of uncertainty of air shower predictions[2,3].

In this article, we will discuss changes in the hadronic model predictions after LHC data and

their consequences on air shower observables. In the first section, we will explain the so-called Heitler model to extract from a simple toy model the main hadronic observables which drive the development of air showers. We will then compare the results of the hadronic interaction models with LHC data for such observables. Finally using detailed Monte Carlo simulations done with CONEX [4], the new predictions for $X_{\max}$ and for the number of muons will be presented.

2 Heitler's Model

To qualitatively describe the dependence of shower development on some basic parameters of particle interaction, decay and production, a very simple toy model can be used. Although initially developed for electromagnetic (EM) showers [5] it can also be applied to hadronic showers [6].

2.1 Electromagnetic showers

For simplicity, instead of having three particle types (γ, e^+ and e^-) like in electromagnetic showers, we will consider only one particle with energy E with only one EM interaction producing two new particles with energy $E/2$ after a fixed interaction length of λ_e, see Fig. 1.
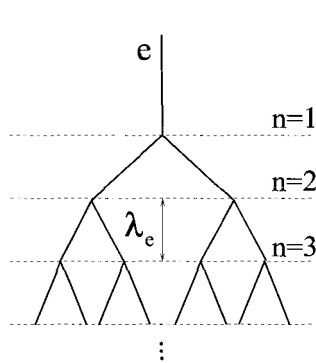

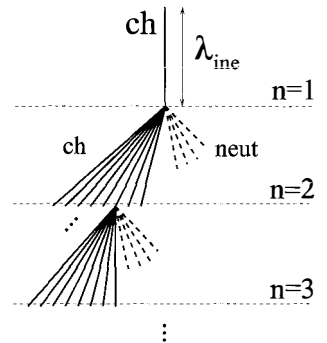Figure 1: Schematic view of electromagnetic cascades.

Figure 2: Schematic view of hadronic cascades. Dashed lines represent neutral particles (π^0) and solid lines charged particles ($\pi^\pm$). Only one charged hadron interaction is shown for each generation.

Denoting with n the number of generations (consecutive interactions), the number of particles at a given depth $X = n \cdot \lambda_e$ follows from

$$N(X) = 2^n = 2^{X/\lambda_e},\tag{1}$$

with the energy E per particle for a given primary energy E_0 being

$$E(X) = \frac{E_0}{2^{X/\lambda_e}}.\tag{2}$$

Defining the critical energy E_c (~ 85 MeV in air) as the energy below which energy loss processes dominate over particle production, one can make the assumption that the shower maximum is reached at a depth at which the energy of the secondary particles reaches E_c. Then two main shower observables are given by

$$N_{\max} = \frac{E_0}{E_c} \quad \text{and} \quad X_{\max}^e(E_0) \sim \lambda_e \cdot \ln\left(\frac{E_0}{E_c}\right).\tag{3}$$

This simplified picture does not reproduce the detailed behavior of an EM shower, but two important features are well described: the number of particles at shower maximum is proportional to E_0 and the depth of shower maximum depends logarithmically on the primary energy E_0.

2.2 Hadronic showers

Generalizing this idea, a hadronic interaction of a particle with energy E is assumed to produce n_{tot} new particles with energy E/n_{tot}, two thirds of which are charged particles n_{ch} (charged pions) and one third are neutral particles n_{neut} (neutral pions), as shown Fig. 2. Neutral particles decay immediately into EM particles ($\pi^0 \to 2\gamma$). After having travelled a distance corresponding to the mean interaction length λ_{ine}, charged particles re-interact with air nuclei if their energy is greater than some typical decay energy E_{dec}.

Shower maximum

Even in an air shower initiated by a hadron, most of the energy is carried by EM particles ($\sim 90\%$ for $n = 6$). Hence the depth of shower maximum is given by that of the EM shower component, X_{max}^e. As the first hadronic interaction produces EM particles of energy $\sim E_0/n_{tot}$ one gets

$$X_{max}(E_0) \quad \sim \quad \lambda_{ine} + X_{max}^e(E_0/n_{tot}) \tag{4}$$

$$\sim \quad \lambda_{ine} + \lambda_e \cdot \ln\left(\frac{E_0}{n_{tot}E_c}\right), \tag{5}$$

where λ_{ine} is the hadronic interaction length. This simplified expression for the depth of maximum neglects the EM sub-showers initiated by hadrons of later generations. The inclusion of higher hadronic generations does not change the structure of Eq. (5), only the coefficients change (see, for example,[7]).

Muon component

To keep the picture simple, we assume that all charged hadrons decay into muons when their energy reaches E_{dec}. In a real shower, this limit can be seen as the characteristic energy where interaction length and decay length of charged pions are similar (about 150 GeV for pions). By construction, charged particles will reach the energy $E_{dec} = \frac{E_0}{(n_{tot})^n}$ after n interactions. Since one muon is produced in the decay of each charged particle, we get

$$N_\mu = n_{ch}^n = \left(\frac{E_0}{E_{dec}}\right)^\alpha, \tag{6}$$

with $\alpha = \ln n_{ch}/\ln n_{tot} = 1 + \ln R/\ln n_{tot} \approx 0.82\ldots0.95$[7] where $R = n_{ch}/n_{tot} < 1$. The number of muons produced in an air shower depends not only on the primary energy and air density, but also on the total particle multiplicities and in a much more sensitive way[8] of the charged over all particle ratio of hadronic interactions.

It should be kept in mind that the parameters of the model are only effective quantities and are not identical to the respective quantities measured at accelerators. In particular, the approximation of all secondary particles carrying the same energy is only motivated by the fact that it allows us to obtain simple, closed expressions. The well-known leading particle effect, typically quantified by the (in)elasticity of an interaction, can be implemented in the model[6] but will not be considered here.

3 Hadronic Interaction Models and LHC data

It is clear that such a model is only giving a very much over-simplified account of air shower physics. However, the model allows us to qualitatively understand the dependence of many air shower observables on the characteristics of hadronic particle production. Accordingly the parameters of hadron production being most important for air shower development are the
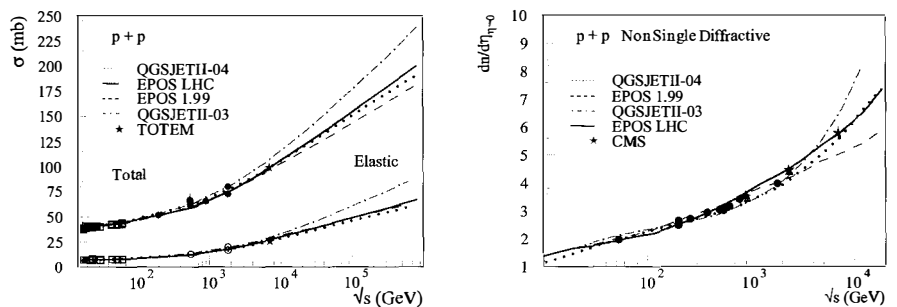
Figure 3: Total and elastic p-p cross section from [18] and LHC measurements by the TOTEM experiment [15] (stars) (left-hand side) and particle density at $\eta = 0$ for non single diffractive events (NSD) from old experiments and from CMS experiment [19] (stars) as a function of center of mass energy. Simulations are done with EPOS LHC (full line), QGSJETII-04 (dotted line), EPOS 1.99 (dashed line) and QGSJETII-03 (dashed-dotted line).

cross section (or mean free path), the multiplicity of secondary particles of high energy, and the production ratio of neutral to charged particles. Until the start of LHC, these parameters were not well constrained by particle production measurements at accelerators. As a consequence, depending on the assumptions of how to extrapolate existing accelerator data, the predictions of hadronic interaction models differ considerably.

There are several hadronic interaction models commonly used to simulate air showers. Here we will focus on the two high energy models which were updated to take into account LHC data at 7 TeV: QGSJETII-03 [9,10] changed into QGSJETII-04 [11] and EPOS 1.99 [12,13] replaced by EPOS LHC [14]. There is no major change in these models but in addition to some technical improvements, some parameters were changed to reproduce TOTEM [15] cross sections. Both are based on Gribov-Regge multiple scattering, perturbative QCD and string fragmentation. The former versions reproduce accelerator data and even first LHC data reasonably well [16] and Figs. 3 and 4 but predict different extrapolations above $E_{cms} \sim 1.8$ TeV ($E_{lab} \sim 10^{15}$ eV) that lead to very different results at high energy [3,17] which can be improved using LHC data.

3.1 Cross section

As shown in eq. 5, the cross section is very important for the development of air showers and in particular for the depth of shower maximum. As a consequence, the number of electromagnetic particles at ground is strongly correlated to this observable (if the shower maximum is closer to ground, the number of particles is higher).

The proton-proton scattering total cross section is usually used as an input to fix basic parameters in all hadronic interaction models. Therefore it is very well described by all the models at low energy, where data exist [20]. And then it diverges above 2 TeV center-of-mass (cms) energy because of different model assumptions. As shown on Fig. 3 left-hand side the new point measured by the TOTEM experiment at 7 TeV reduces the difference between the models by a factor of 5 (50 to 10 mb) at the highest energy. In all the figures EPOS LHC is represented by a full (blue) line, QGSJETII-04 by a dotted (red) line, EPOS 1.99 by a dashed (black) line and QGSJETII-03 by a dashed-dotted (green) line.

3.2 Multiplicity

According to eq. 5, the multiplicity plays a similar kind of role as the cross section, but with a weaker dependence (log). On the other hand, the predictions from the models had much larger
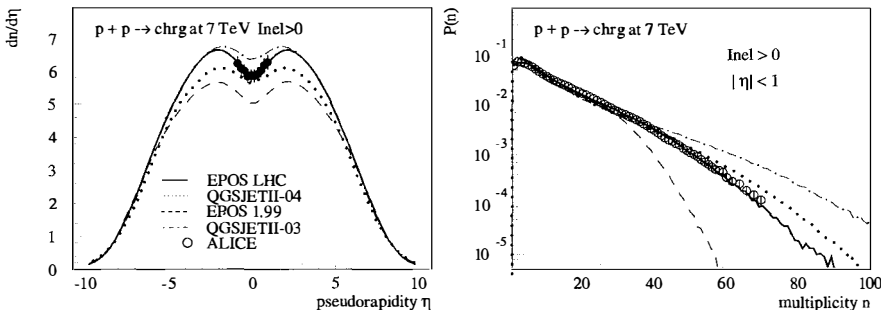
Figure 4: Pseudorapidity distribution $dN/d\eta$ for events with at least one charged particle with $|\eta| < 1$ (left-hand side) and corresponding multiplicity distribution (right-hand side) for p-p interactions at 7 TeV. Simulations with EPOS LHC (full line), QGSJETII-04 (dotted line), EPOS 1.99 (dashed line) and QGSJETII-03 (dashed-dotted line) are compared to data points from ALICE experiment [22].

differences for the multiplicity compared to the cross section. As shown Fig. 3 right-hand side, the particle density at mid-rapidity is well reproduced by all the models up to 2 TeV where Tevatron data [21] constrain the results, but at the highest energies (not shown), the difference can be as high as a factor of 10. After re-tuning at 7 TeV to be compatible with CMS data [19] or ALICE data [22] on Fig. 4, the difference is now negligible. On the right-hand side of Fig. 4, we can see that not only the averaged multiplicity had been changed after re-tuning, but the fluctuations are now very similar for QGSJETII-04 and EPOS LHC. This will be important for the fluctuations of the air shower maximum.

So for both cross section and multiplicity, when the models are constrained by LHC data up to 7 TeV, the extrapolation to the highest energy is not so different any more. This will have a strong impact on X_{max} uncertainty in air shower simulations.

3.3 Baryon production

Another important observable for EAS is the number of muons reaching the ground. Using eq. 6 and the definition of α and R, it has been shown in [8] that the number of (anti)baryons plays an important role in the value of R especially if we take into account the leading particle effect. As a consequence the number of muons in EAS is sensitive to the number of (anti)baryons produced in the hadronic interactions and it is important to check the production of such particles in LHC data.

Both ALICE [23] and CMS [24] experiments published very nice results on identified spectra used to constrain models used for air shower simulations. As shown in Fig. 5 left-hand side, these data helped a lot to reduce the differences between the models especially because it could resolve an ambiguity on the phase space used to produce some anti-proton over pion ratio with Tevatron data at 1.8 TeV. LHC data are much better defined and can be used to constrain the production of baryon pairs at mid-rapidity (largely dominated by string fragmentation).

It is important to notice that not only (and not all) (anti)baryons are entering in the definition of the ratio R. All particles which do not decay into an electromagnetic particle can play a similar role and keep the energy of the shower into the hadronic channel to produce muons. For instance in QGSJETII-04 the newly introduced ρ^0 resonance as excited state of the pion remnant in pion interactions has a very strong influence on the muon production. Since forward π^0, transferring a lot of energy in the electromagnetic channel, are replaced by particles which decay in charged pions, the energy is kept in the hadronic channel. This is clearly illustrated
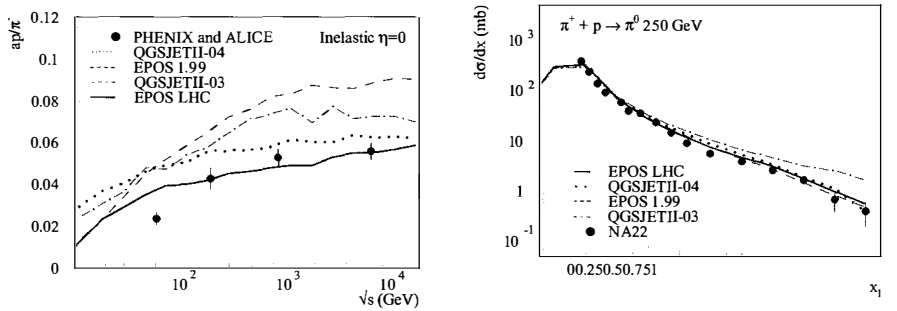
43

Figure 5:   Measurement of pion over anti-proton ratio at $y = 0$ for p-p collisions by ALICE and PHENIX [23] experiments (left-hand side) as a function of center of mass energy and measurement of the π^0 longitudinal momentum fraction distribution by NA22 experiment [25,26] (right-hand side) for π-p interactions at 250 GeV lab. Simulations are done with EPOS LHC (full line), QGSJETII-04 (dotted line), EPOS 1.99 (dashed line) and QGSJETII-03 (dashed-dotted line).

by the Fig. 5 right-hand side where we can see that QGSJETII-04 reproduce nicely π^0 forward spectra while QGSJETII-03 producing no ρ^0 had too hard π^0 spectra. The leading ρ^0 production was already in EPOS 1.99, being one source of difference between the 2 models. On the other hand in EPOS 1.99 another process producing forward (anti)baryons was missing at high energy. As a consequence the reduced rate of (anti)baryons production at mid-rapidity is compensated by more forward (anti)baryons production which is even more important for muon production. Unfortunately there is very little data to constrain this production channel especially in collider experiments. NA61 and LHCf data may help to constrain this process in the future.

4   EAS Simulations

Using the air shower simulation package CONEX and the new versions of the high-energy hadronic interaction models, we can get an estimate of the resulting uncertainties. In the following EAS simulation results using EPOS LHC and QGSJETII-04 are presented and compared to former results using QGSJETII-03 and EPOS 1.99.

As shown in Fig. 6 left-hand side, the mean depth of shower maximum, X_{max}, for proton and iron induced showers simulated with CONEX is still different for EPOS LHC and QGSJETII-04. But now the elongation rate (the slope of the mean X_{max} as function of the primary energy) is the same in both cases while EPOS 1.99 had an elongation rate larger than QGSJETII-03. The difference between the 2 models is a constant shift of about $20g/cm^2$ (close to the experimental systematic error in PAO [27]) while before the difference were increasing up to $50g/cm^2$ at the highest energies

This is very important to study the primary cosmic ray composition. If the models converge to a similar elongation rate, it will allow us to have a more precise idea on possible changes in composition at the "ankle" for instance where the PAO measured a break in the elongation rate of the data.

Concerning the number of muons at ground (for $40°$ inclined shower at the height of 1500 m), the difference between the new QGSJETII-04 and the old QGSJETII-03 is even more impressive. We can see on Fig. 6 left-hand side that QGSJETII-04 predicts now about the same number of muons than EPOS 1.99 which is about 20% more than QGSJETII-03. It is due to the change in baryon, strangeness and mostly resonance production as described in section 3.3.
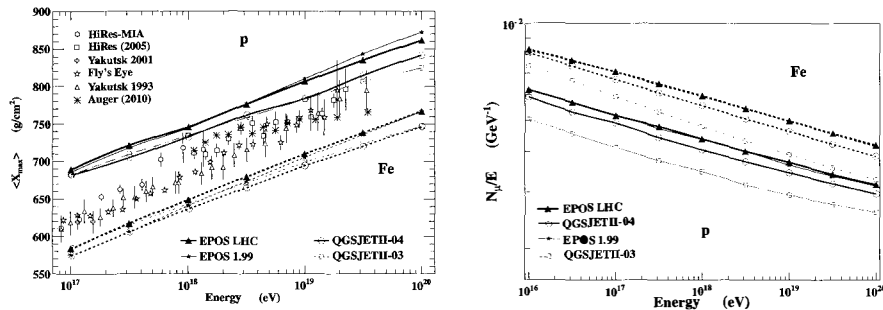
Figure 6: Mean X_{max} (left-hand side) and mean number of muons at ground divided by the primary energy (right-hand side) for proton and iron induced showers are shown as a function of the primary energy for different high-energy hadronic interaction models, full lines for proton and dashed lines for iron with full triangles for EPOS LHC, open squares for QGSJETII-03, open circles for QGSJETII-04, and full stars for EPOS 1.99. Refs. to the data of mean X_{max} can be found in [27] and [28].

Concerning the predictions of EPOS LHC, the number of muons is very similar to the one in EPOS 1.99 because of the leading baryon production compensating the reduction of (anti)aryon production at mid-rapidity. So, even if the number of muons is much more similar now for the two most recent hadronic models, there is still an uncertainty of about 10% and furthermore the energy spectrum of the muons at ground is different between the models. This is important for the calculation of the missing energy for fluorescence detection. The average energy of the muons is larger in QGSJETII-04 than in EPOS resulting in a sligthly larger (1% to 2%) missing energy correction in QGSJETII-04 (same value for EPOS LHC and EPOS 1.99).

5 Summary

Using a simple cascade model, it is possible to find the main parameters of hadronic interactions that influence air shower predictions. For the mean depth of shower maximum, $\langle X_{max} \rangle$, these parameters are the inelastic cross sections, the secondary particle multiplicity, and the inelasticity (not studied here). Using recent LHC data at 7 TeV it is possible to reduce the uncertainty in the extrapolation of the hadronic interaction models used for EAS simulations. Using pre- and post-LHC versions of the QGSJETII and EPOS models, it has been showed that the difference in multiplicity between these models has been reduced by a factor of 5 at the highest energy, resulting in a very similar elongation rate. There is still a systematic shift in X_{max} of about $20g/cm^2$ due to remaining differences in the multiplicity (and elasticity) of the models. This uncertainty is comparable to the experimental uncertainty in the measurement of X_{max}. As a consequence the interpretation of the data using post-LHC data will be more reliable especially concerning the possible change in mass composition with energy as summarized in [29].

For the number of muons, the ratio between particles producing hadronic sub-showers and the total number of particles is very important. LHC data are important to constrain (anti)baryon and strangeness production at mid-rapidity. Lower energy data of fixed target experiment are also important to measure forward production of π^0 for instance. Taking into account both aspect, the new version of the QGSJETII and EPOS models predict very similar results close to EPOS 1.99 model but with harder spectrum.

The difference between EPOS 1.99 and the preliminary results of EPOS LHC is not very large because most of the changes are taking place at mid-rapidity. This phase space is good to test the physics of the model but is not very important for air shower development. A contrario, large differences between QGSJETII-03 and QGSJETII-04 are observed. With a

larger $\langle X_{max} \rangle$ the average mass is heavier than before at Auger energies. Since the number of muons increased by about 20% and taking into account this larger average mass, the difference with the number of muons observed by PAO will be reduced significantly.

1. J. Abraham, et al. [Pierre Auger Observatory], *Nucl. Instrum. Meth.* **A523**, 50–95 (2004).
2. J. Knapp, D. Heck, and G. Schatz, Wissenschaftliche Berichte FZKA 5828, Forschungszentrum Karlsruhe (1996).
3. J. Knapp, D. Heck, S. J. Sciutto, M. T. Dova, and M. Risse, *Astropart. Phys.* **19**, 77–99 (2003), [astro-ph/0206414].
4. T. Bergmann, et al., *Astropart. Phys.* **26**, 420–432 (2007), [astro-ph/0606564].
5. W. Heitler, *Quantum Theory of Radiation*, Oxford University Press, Oxford, 1944, 2nd edition.
6. J. Matthews, *Astropart. Phys.* **22**, 387–397 (2005).
7. J. Alvarez-Muniz, et al. *Phys. Rev.* **D66**, 033011 (2002).
8. T. Pierog, and K. Werner, *Phys. Rev. Lett.* **101**, 171101 (2008).
9. S. Ostapchenko, *Phys. Rev.* **D74**, 014026 (2006), [hep-ph/0505259].
10. S. Ostapchenko, *Phys. Lett.* **B636**, 40–45 (2006), [hep-ph/0602139].
11. S. Ostapchenko, Phys. Rev. D **83** (2011) 014018 [arXiv:1010.1869 [hep-ph]].
12. K. Werner, F.-M. Liu, and T. Pierog, *Phys. Rev.* **C74**, 044902 (2006), [hep-ph/0506232].
13. T. Pierog, and K. Werner, *Nucl. Phys. Proc. Suppl.* **196**, 102–105 (2009), [arXiv:0905.1198 [hep-ph]].
14. T. Pierog, et al., [arXiv:1306.0121 [hep-ph]].
15. T. Čsörgő, et al., [TOTEM Collaboration], *Prog. Theor. Phys. Suppl.* **193**, 180 (2012).
16. D. d'Enterria, R. Engel, T. Pierog, S. Ostapchenko and K. Werner, Astropart. Phys. **35** (2011) 98 [arXiv:1101.5596 [astro-ph.HE]].
17. R. Engel, and H. Rebel, *Acta Phys. Polon.* **B35**, 321–330 (2004).
18. C. Caso, et al., *Eur. Phys. J.* **C3**, 1 (1998).
19. V. Khachatryan, et al. [CMS Collaboration], *Phys. Rev. Lett.* **105**, 022002 (2010), [arXiv:1005.3299 [hep-ex]].
20. H. Jung, et al. (2009), [arXiv:0903.3861 [hep-ph]].
21. F. Abe, et al., *Phys. Rev.* **D41**, 2330 (1990).
22. K. Aamodt, et al., [ALICE Collaboration], *Eur. Phys. J. C* **68**, 345 (2010).
23. M. Chojnacki [ALICE Collaboration], *J. Phys. G* **38** 124074 (2011), [arXiv:1109.6744 [hep-ex]].
24. S. Chatrchyan, et al., [CMS Collaboration], [arXiv:1207.4724 [hep-ex]].
25. M. R. Ataian, et al., [EHS-NA22 Collaboration], *Z. Phys. C* **54** 247 (1992).
26. N. M. Agababyan, et al., [EHS-NA22 Collaboration], *Z. Phys. C* **46** 387 (1990).
27. J. Abraham, et al. [Pierre Auger Observatory], *Phys. Rev. Lett.* **104**, 091101 (2010), [arXiv:1002.0699 [astro-ph.HE]].
28. J. Blümer, R. Engel, and J. R. Hörandel, *Prog. Part. Nucl. Phys.* **63**, 293–338 (2009), [arXiv:0904.0725 [astro-ph.HE]].
29. K.-H. Kampert and M. Unger, Astropart. Phys. **35** (2012) 660 [arXiv:1201.0018 [astro-ph.HE]].